MILLIMAN WHITE PAPER

Where is Europe's next flash flood?

Quantifying extreme precipitation and flash flood risk in Europe with extreme value theory

Matt Chamberlain, FCAS, CSPA, MAAA
Fernando Mierzejewski, PhD
Jan Thiemen Postema
Thomas van der Valk
Menno van Wijk, AAG

Milliman

In this white paper we apply extreme value theory (EVT) to assess the risk of extreme precipitation events in Europe.

Europe has witnessed a sharp uptick in catastrophic flash flood losses, punctuated by record-breaking downpours such as those in Valencia in 2024 and Western Europe in 2021. The amounts of rainfall experienced were higher than anticipated. This raises the question: In which European regions are similar events most likely to occur?

We have applied EVT to rainfall data over a wide range of European weather stations to derive precipitation levels for different return periods based on what statistical theory tells us. Here we use an automated method to estimate extreme return levels at scale, supplemented by manual methods to improve fits where necessary. This white paper distills our findings and demonstrates how insurers and governmental agencies can harness EVT to structure parametric insurance covers, sharpen solvency assessments, and guide resilient infrastructure investment.

Flash flood risk

RECENT HISTORIC EVENTS

Recent history has shown multiple extreme rainfall events occurring in Europe. We single out the following:

- 2024 Spanish floods: As a result of a cold drop (known in Spanish as a DANA[1]), 771 mm of rain was recorded at weather station Turis in Valencia, Spain, on 29 October 2024. This was the second-highest level of rainfall recorded in 24 hours in Spain, after 817 mm in Oliva (in the Valencia region as well) on 3 November 1987.[2] Floods also occurred in other Spanish regions, such as around Barcelona in early November 2024. The 2024 floods led to 232 fatalities and €10.7 billion in economic loss, of which €3.5 billion was insured.[3]
- 2024 Central European floods: Storm Boris caused extreme rainfall throughout Central Europe in the period 14–21 September. Northern regions in Czechia accumulated a three-day total of 442 mm,[4] while in other areas amounts equal to five times the usual monthly amounts for September were recorded. The resulting floods led to 27 fatalities and an economic loss of €4.2 billion, of which €1.9 billion was insured.[5]
- 2021 Western European floods: In the period 12–16 July, extreme precipitation was observed in Western Europe, most notably in Germany. Weather station Köln-Stammheim tallied 154 mm of rain in 24 hours, exceeding the previous daily record for the city of 95 mm.[6] Throughout Europe, 243 fatalities were recorded as a result of the floods. The economic losses amounted to €46 billion,[7] making it Europe's costliest natural disaster that year.[8]

These episodes reveal a recurrent pattern: unexpectedly extreme rainfall over confined windows (hours to days) that overwhelms urban drainage and river networks, leading to flash floods and causing multiple fatalities and severe economic losses. The extent to which the rainfall in these events could have been expected can be analyzed statistically with EVT.

Introduction to EVT

WHAT IS EVT?

Extreme value theory is the branch of statistics that isolates and models the rarest, most severe observations in a stochastic process. Therefore, EVT is one of the most important tools when one is interested in investigating tail behavior, which is exactly where flash flood risk resides.

EVT includes two important theorems concerning the limiting distribution of independent, identically distributed (iid) variables. These are analogous to the well-known central limit theorem for means, but concern behavior in the tail of the distribution. These theorems form the basis for the two most common methods of applying EVT.

BLOCK MAXIMA METHOD

The block maxima method[9] concerns analysis of extreme values for uniform blocks from a dataset. For instance, when one analyzes a dataset containing daily observations of the quantity of interest, block maxima could focus on the maxima for each month. The monthly maximum observations are then called the block maxima, which, combined, form an approximation of the tail of the distribution of the entire dataset.

According to the block maxima theorem, or the Fisher-Tippett-Gnedenko theorem,[10] the distribution of block maxima of any series of iid random variables asymptotically converges to a generalized extreme value (GEV) probability distribution as the number of elements in the series increases.

The parameters of the GEV distribution can then be determined from the block maxima, providing the tail distribution.

PEAK OVER THRESHOLD METHOD

Alternatively, one could focus on all values exceeding a certain threshold value, instead of taking the maximum values from each block. In such an approach, the values higher than the threshold are called exceedances over threshold and would by definition form the tail of the distribution of the dataset.

According to the peak over threshold (POT) theorem, or the Pickands-Balkema-De Haan theorem,[11] the distribution of the exceedances over threshold of any series of iid random variables asymptotically converges to a generalized Pareto distribution (GPD) as the number of elements in the series increases.

The parameters of the GPD distribution can then be determined from the exceedances over threshold. Like the block maxima method, this also provides the tail distribution. The methods have different advantages and disadvantages. The POT method requires more granular data than the block maxima method (which requires just one value per block), but uses the data more efficiently and therefore may result in narrower confidence intervals.

Application of EVT to precipitation data

DATA DESCRIPTION

The precipitation data in our analysis comes from the National Centers for Environmental Information (NCEI), which provides environmental datasets, including daily climate records from meteorological stations worldwide. Specifically, we utilize the Global Historical Climatology Network daily (GHCNd) database,[12] with a particular focus on European stations. These data are subject to a number of quality assurance reviews.

The initial dataset consisted of 2,398 stations spanning nearly all European countries. During data preparation, we filtered stations to retain only those with at least 65 years of observations, less than 10% missing data, and currently still gathering data. This filtering process reduced our set to 612 stations.

HOMOGENIZATION

We then further filtered the dataset via the homogenization method described in STOWA's 2019 report.[13] Here, homogeneity is assessed on a series constructed by subtracting a region average from the yearly number of wet days for a particular station, as stations within a region are assumed to exhibit similar patterns in the number of wet days over time. Regions are defined using a K-means clustering algorithm based on the locations of the weather stations. Figure 1 illustrates how our districts are geographically located.

FIGURE 1: GEOGRAPHIC CLUSTERING OF WEATHER STATIONS BASED ON K-MEANS ALGORITHM

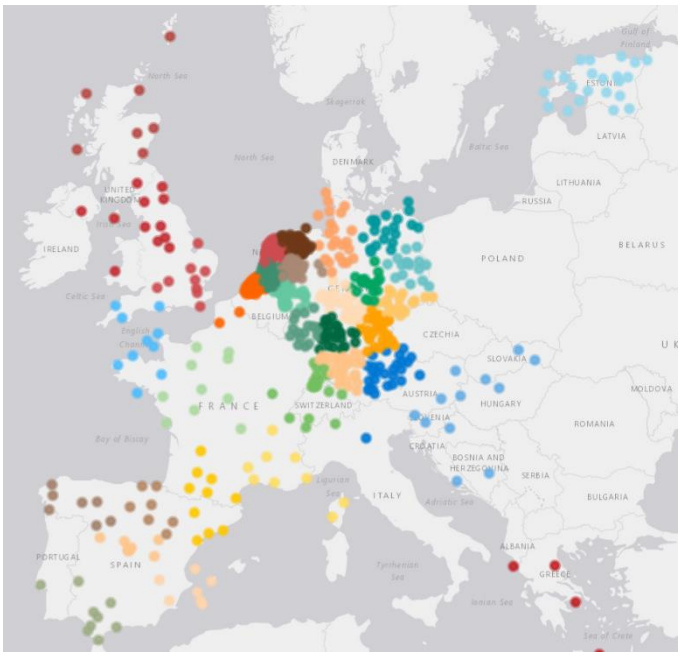

The regions are necessary to help distinguish climate-related trends and fluctuations from inhomogeneities. Using the region-average-corrected series, four homogeneity tests, as specified in Wijngaard et al. (2003),[14] are performed. We have classified stations as useful if at most one test indicates inhomogeneity. If two or more tests indicate inhomogeneity, the stations are removed from the dataset. A significance level of 5% was chosen for all statistical tests.

For our sample of 612 stations, the tests classified 553 as useful, while the other 59 stations had more than one test indicating inhomogeneity and were therefore removed. Our analysis therefore proceeds with the reduced subset of 553 stations.

METHODOLOGY

Choice of method

As discussed earlier, the two most common approaches for applying EVT are the block maxima method and the POT method. While both methods have their advantages and disadvantages, we selected the POT method, based on two considerations.

First, as previously mentioned, the POT method uses the data more efficiently. If a block has many extreme values, the block maxima method only uses the largest value, while the POT method uses all the extreme values. Second, if we select a smaller block (perhaps in an effort to mitigate this first limitation), we risk introducing issues arising from seasonality. For example, if we use monthly blocks but rainfall patterns vary at different times of year then the distribution for each block is no longer iid. The POT method, however, introduces additional complexity, namely, adequate threshold selection.

Threshold selection

EVT is only valid in the tail—that is, above some high threshold. But how should that threshold be selected? Visual methods, such as quantile-quantile (QQ) plots and mean excess plots, have been developed, as well as quantitative metrics such as the Kolmogorov-Smirnov[15] and Cramér-von Mises[16] test statistics.

However, since these approaches require evaluation by an analyst for each station, it is difficult to apply them at scale. This is true in our situation, where we are working with hundreds of weather stations. To overcome this problem, we make use of an automated threshold selection procedure.

Several automated threshold selection procedures have been developed, including the power law method[17] and double bootstrapping (DBS) methods[18] based on sampling (bootstrapping). For our analysis, we evaluated multiple methods and selected the DBS kernel method.

For every weather station, we calibrated the GPD distribution on the exceedances over threshold, using the automated threshold from the DBS kernel method. For certain cases where the resulting fit was deemed inadequate, we used manual threshold selection. We discuss this approach in more detail later in this paper.

IMPLEMENTATION AND RESULTS

We implemented the methodology described above in an interactive web app, using the R package Shiny. We also made use of code developed in the R ismev package,[19] an implementation of the code from Coles (2001).[20]

Results using automated threshold selection

In addition to the parameters of the GPD distribution for each weather station determined by the automated threshold selection method, we obtain estimated return levels for different return periods,[21] confidence intervals associated with those return levels, and several diagnostic plots.

Figure 2 shows the return levels corresponding to the 100-year return period for weather stations where the 95% confidence interval is sufficiently narrow. Lighter blue dots correspond to relatively low return levels, while darker blue dots correspond to higher return levels. The patterns we observe are geographically consistent and give relevant insight in the high-risk areas.

- While the United Kingdom is relatively prone to flash floods, with multiple events having occurred in the past few years, the return levels resulting from our analysis are below 10 cm.
- Similarly, homogeneous and relatively low return levels are observed across the Netherlands. Here, the return levels are on average well below 10 cm. The highest return levels are observed in the south of the country, with the highest value being observed in Ubachsberg. The return level there is around 11 cm, which is higher than the extreme event that occurred in July 2021.
- Return levels in Northern Europe are higher when moving east, which is consistent with more frequent extensive rainfall historically recorded in Central Europe. Return levels between 10 and 15 cm are not unusual in Germany.
- In the Alps region, return levels become higher, approaching and sometimes exceeding 20 cm.
- In Southern Europe, across the Mediterranean coasts, the return levels are highest. For many stations, return levels around 25 cm are obtained, while for Valencia the return level exceeds 30 cm.
- In the north of the Iberian Peninsula, return levels are comparable to the Alps region, while in the Spanish midlands, return levels are comparable to those in the Netherlands.

The relative risk between regions is similar when looking at higher return periods. Hence, the combination of historical data and EVT shows us that, for the stations in our dataset, the risk of extreme precipitation is highest across the Mediterranean coast.

FIGURE 2: 100-YEAR RETURN LEVELS (IN CM) PER WEATHER STATION

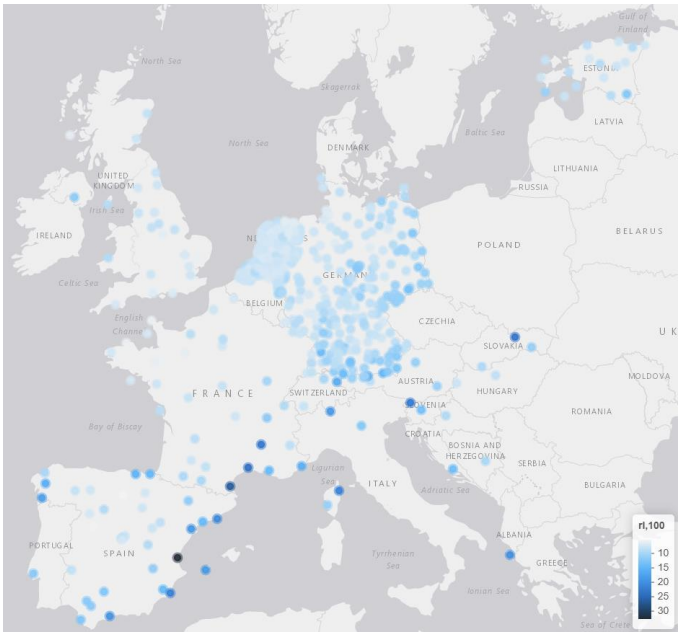

Source: Image generated using Milliman analysis and R package leaflet.

In addition to the analysis of absolute return levels, we also compared the 100-year return levels from the fitted distributions to the historical maximum observed in the dataset. This can be seen as a simple evaluation of the fit of the far end of the tail, given that the dataset contains around 100 years of data for most weather stations.

The results are shown in Figure 3, where a negative number (orange dot) indicates a higher empirical maximum than the model fit, while a positive number (green dot) indicates that the model predicts a higher return level than observed in the data so far. The darker the dot, the bigger the difference is.

The weather stations depicted by green dots are especially interesting, as the results imply that heavier rainfall than ever seen before is possible at these locations. We see no areas with consistent model over- or underestimation; however, absolute differences are, as expected, bigger in areas where return levels are higher. For instance, at the weather stations Valencia (Spain)[22] and Perpignan (France), estimated return levels are high, as shown in Figure 2, and also considerably higher than the historical maximum, as shown in Figure 3. In other words, these locations are expected to be more at risk for extreme events that have not occurred before.

FIGURE 3: DIFFERENCES BETWEEN 100-YEAR RETURN LEVELS AND HISTORICAL MAXIMUM (IN CM) PER WEATHER STATION

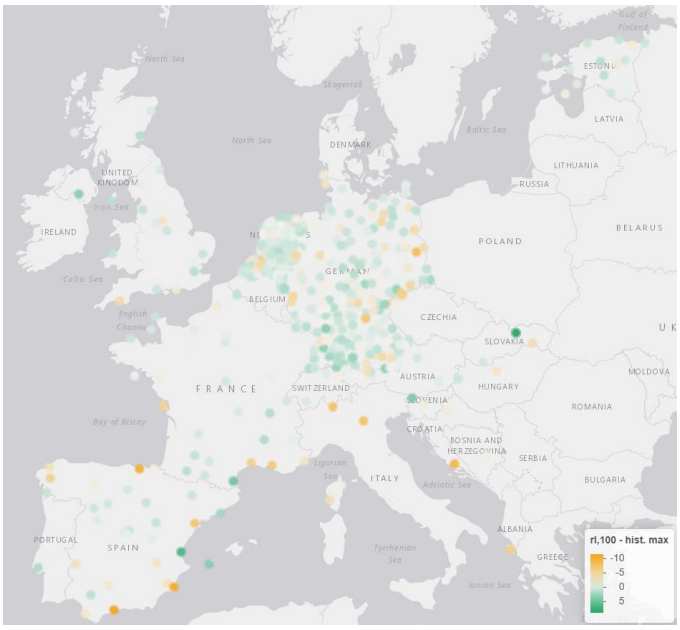

Source: Image generated using Milliman analysis and R package leaflet.

To assess the quality of the fitted distributions, we considered several approaches. One commonly used is the QQ plot. When the points in the QQ plot land approximately on a straight line through the origin, the fitted distribution closely resembles the data. When points land above the straight line, the model underestimates actual precipitation, and when points land below the straight line, the model overestimates precipitation. Figure 4 shows an example of a weather station with a good fit.

FIGURE 4: QQ PLOT FOR WEATHER STATION DRESDEN-HOSTERWITZ (GERMANY)

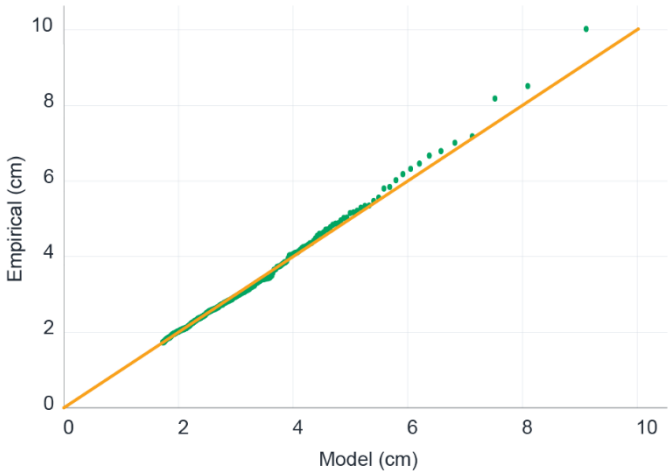

We have also used the QQ comparison for quantitative evaluation of the model fits. In Figure 5, we map the sum of absolute differences between model and empirical quantiles, relative to the corresponding empirical quantile, over all empirical points corresponding to a fitted return period exceeding 20 years. Darker green dots correspond to small summed absolute differences, while the differences increase for lighter green, yellow, and orange dots.

FIGURE 5: QQ PLOT ABSOLUTE DEVIATIONS

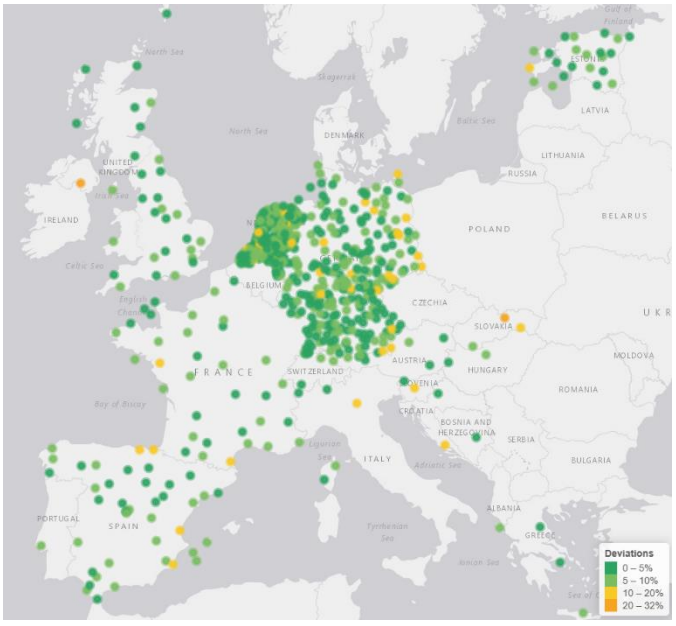

Source: Image generated using Milliman analysis and R package leaflet.

As can be seen from the histogram in Figure 6, for more than 95% of the weather stations the deviations are below 20%, indicating an acceptable to good fit. For more than 60% of stations the deviations are below 10%.

For the extreme cases with deviations over 20% (concerning just over 4% of stations), we investigated whether manual threshold selection could improve the model fit.

FIGURE 6: HISTOGRAM OF QQ PLOT DEVIATIONS

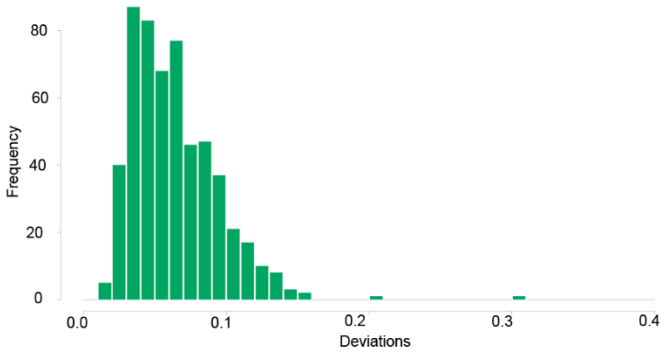

Results using manual threshold selection

In the classical POT approach, the threshold above which the GPD distribution is fit results from manual selection. While we have shown that automated threshold selection yields satisfactory fits for most stations in our dataset, improvements could be possible by applying manual threshold selection.

In Figure 7, we show the QQ plot of the automated threshold GPD fit for the weather station Boskoop in the Netherlands. This is an example of a weather station that did not fit well using the automated threshold selection. The selected threshold was 1.35 cm, meaning that the model was fit on all observations exceeding 1.35 cm. The plot shows that the most extreme historical observations are higher than predicted according to the model; that is, the model seems to underestimate the tail of the distribution.

FIGURE 7: QQ PLOT AUTOMATED THRESHOLD GPD FIT—BOSKOOP, NL

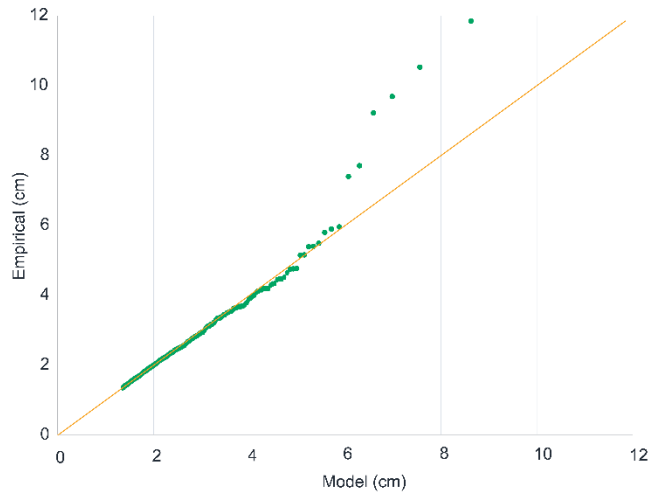

In fact, we even see in Figure 8 that the observations fall outside the 95% confidence interval that follows from our model fit. This can be seen as additional confirmation that this fit requires more attention.

FIGURE 8: RETURN LEVEL PLOT AUTOMATED THRESHOLD GPD FIT—BOSKOOP, NL

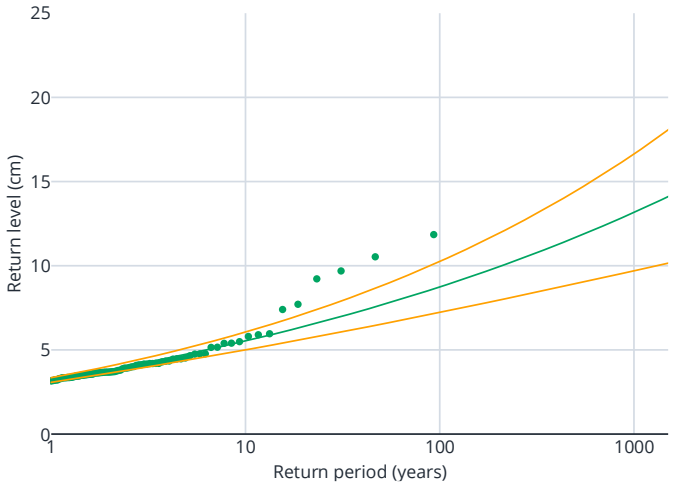

In our manual selection of most appropriate threshold, we first consider the mean excess plot, shown in Figure 9. The way to use a mean excess plot for threshold selection is to look for the lowest value of the threshold u (plotted on the x-axis) for which the mean excess (plotted on the y-axis) shows a linear relation in u, while maintaining a relatively narrow confidence interval (plotted by the dashed lines).

FIGURE 9: MEAN EXCESS PLOT—BOSKOOP, NL

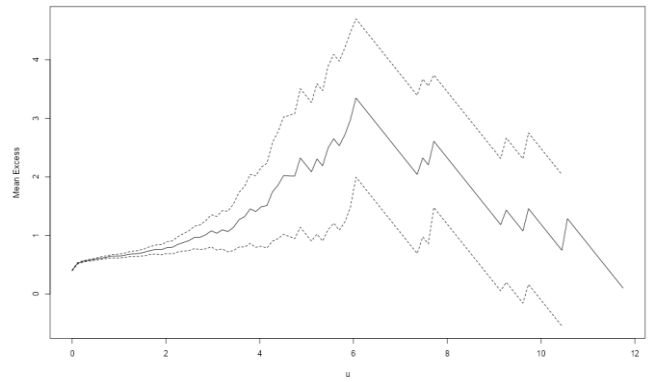

In addition, we plot the Cramér-von Mises test statistic in relation to the threshold in Figure 10. In this graph, our optimal threshold would be in a range where the statistic is low and would remain at a similar level when increasing the threshold.

FIGURE 10: CRAMÉR-VON MISES TEST STATISTIC IN RELATION TO THRESHOLD—BOSKOOP, NL

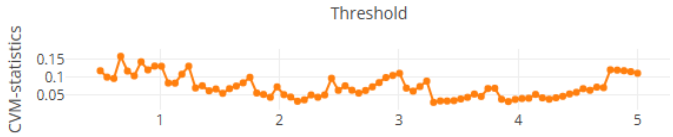

From both figures, we infer that the automated threshold of 1.35 cm appears to be too low for this weather station. The mean excess plot in Figure 9 does not yet show a linear relation from threshold 1.35 cm onward, while the Cramér-von Mises test statistic in Figure 10 is still decreasing for higher threshold values. Based on both plots, we choose a manual threshold of 3.28 cm. This leads to the QQ plot in Figure 11.

FIGURE 11: QQ PLOT MANUAL THRESHOLD GPD FIT—BOSKOOP, NL

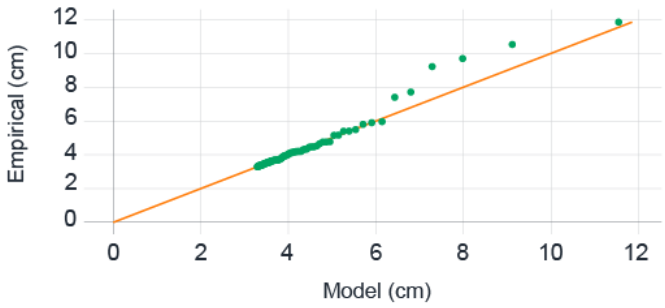

Compared to the QQ plot for the automated threshold GPD fit (Figure 7), we can see that the model fit has indeed improved for this manually selected threshold, as the most extreme data points are now plotted much closer to the straight line through the origin. We also see in Figure 12 that the observations now fall within the 95% confidence interval of our model. However, we also see that the increase of threshold compared to the initial model fit leads to wider confidence intervals, especially for return periods beyond around 200 years.

FIGURE 12: RETURN LEVEL PLOT MANUAL THRESHOLD GPD FIT—BOSKOOP, NL

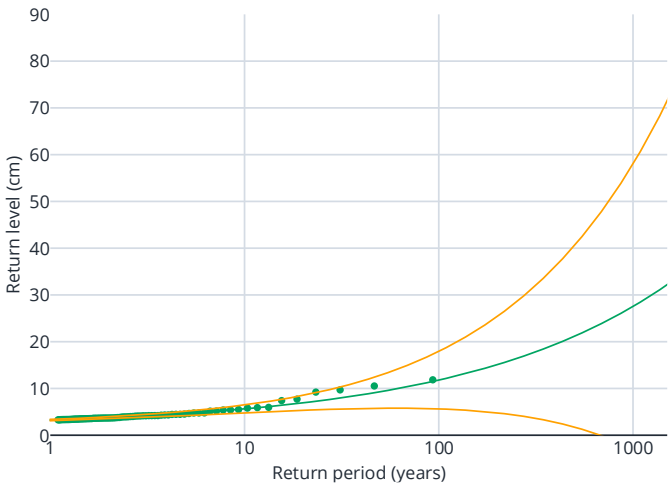

When expressed in our metric of absolute QQ plot deviations introduced earlier, our fit improved from a 28% deviation on the automated threshold GPD fit to a 14% deviation.

The results from the automated and manual threshold selections combined show that we have developed a scalable framework in which we can efficiently fit extreme value distributions for a large number of points of interest (weather stations in our application), while manual threshold selection can be used as an additional measure to improve fits where the fit from the automated threshold selection procedure is not satisfactory.

BACKTEST

As an additional measure for model evaluation, we performed a backtest on an extreme historic event. For this, we performed a separate calibration of the model using data until end of 2020, to exclude the events that occurred in the years 2021–2024. At a high level, we see that return levels are stable. Some differences are observed in the stations in eastern Germany and Slovakia, which were affected by Storm Boris and other heavy events in 2022 and 2023 as well.

For the Barcelona Airport weather station, we analyzed the impact of the November 2024 extreme rainfall on the model calibration in more detail. On 4 November 2024, 14.42 cm of rainfall was recorded, which led to flooding of the airport and surrounding highways.[23] In the model calibration until the end of 2020, this level of rainfall corresponded to a return period of around 19 years. In the calibration taking the full dataset into account, the corresponding return period is 18.8 years. This shows that the experienced event could have been reasonably expected (on average once every 20 years an event of this magnitude could occur) and factoring it in does not materially change the likelihood of the event, demonstrating robustness.

Practical use cases

PARAMETRIC INSURANCE

Most insurance contracts, especially in the developed world, are indemnity based. This means that a claim can arise only when the insured object is affected by a certain insured event, while the size of the claim is determined by the extent to which the object is damaged. In contrast, parametric insurance is index based, meaning that a claim arises when a predetermined trigger level on a certain index or benchmark is reached. The size of the claim is then derived from a payout scheme. In such a case, the insured loss is therefore independent of actual damage incurred by the beneficiary, speeding up the payout process at the expense of basis risk remaining with the policyholder.

EVT can allow for transparent, objective trigger setting. Based on a calibrated tail distribution and the risk appetite of either the insurer or beneficiary, one can determine at which level or levels of the insured index (e.g., rainfall measured in a certain weather station on a 24-hour basis) a payout occurs. The premium can be determined accordingly.

While in this white paper we focus on precipitation data and flash flood risk, the approach can be used for many other factors as long as sufficient data is available. For instance, drought levels or the size of hailstones can be used as an index for crop insurance, seismic movement can be used as index for earthquake coverages, and wind speeds can be used as an index for property insurance. For all these types of indexes, EVT can be used to fit tail distributions and determine triggers.

SOLVENCY II AND OTHER REGULATORY FRAMEWORKS

EVT can also be used as a tool feeding into regulatory frameworks such as Solvency II, Solvency UK, and the Swiss Solvency Test. As discussed in the previous section, EVT can be applied to many risk drivers such as rainfall, asset returns, lapses, etc. to:

- Benchmark and validate models used for the calculation of capital requirements, such as (vendor) catastrophe models or even the standard formula. EVT return levels can be used as a check on (intermediate) model outputs, either by a model developer or owner, or by an independent model validator as meant under Article 241 of the Solvency II Delegated Acts.[24]
- Generate risk scenarios for own risk and solvency assessment (ORSA), for instance, under different climate-change pathways.

In some cases, EVT could even be directly used for Internal Model calibrations for the Solvency Capital Requirement—that is, the 99.5% Value-at-Risk. However, this would require datasets that exactly relate to the risk or peril in scope, with sufficient history (likely well beyond 100 years) and showing stable behavior (i.e., not containing trends).

GOVERNMENTAL PLANNING AND RESILIENCE

In the public sector, EVT results can be used in urban planning to increase resilience to possible extreme events. We see the following domains of application:

- Infrastructure design: adequately sized culverts, retention basins, and urban drainage based on EVT-inferred rainfall loads for return periods in line with risk appetite.
- Cost-benefit optimization: balance investments in infrastructure versus expected losses, using the tail distribution as calibrated via EVT for estimating the loss curve.
- High-risk zone identification: When using data on a granular level, EVT can be used to identify high-risk zones. In connection with a definition of an unacceptable level of risk, this could lead to identification of areas where building of new property or infrastructure is prohibited.

Likewise, insurers could use these insights to suggest prevention measures to their clients.

Conclusion

In recent history, several floods as a result of extreme rainfall have occurred in Europe. Our analysis, which combines historical data and EVT, shows that for the stations in our dataset, the risk of such events occurring again in the future is highest across the Mediterranean coast.

Furthermore, we have proved that EVT offers a statistically sound and data-efficient pathway to quantify flash flood risk. In addition to the geographical conclusions on risky regions, our Europe-wide study demonstrates:

- Robust and efficient estimation of high-return-period rainfall for a large number of weather stations.
- Transparent diagnostics for quality of fit that signal whether manual intervention is required.
- Direct applicability to parametric insurance design, methods to determine capital adequacy, and public and private sector resilience.

In addition to applying the theory to rainfall data, many other quantities of interest can be identified, thereby increasing the practical relevance of our research.

Solutions for a world at risk™

Milliman leverages deep expertise, actuarial rigor, and advanced technology to develop solutions for a world at risk. We help clients in the public and private sectors navigate urgent, complex challenges—from extreme weather and market volatility to financial insecurity and rising health costs—so they can meet their business, financial, and social objectives. Our solutions encompass insurance, financial services, healthcare, life sciences, and employee benefits. Founded in 1947, Milliman is an independent firm with offices in major cities around the globe.

milliman.com

CONTACT

Matt Chamberlain
Matt.Chamberlain@milliman.com

Fernando Mierzejewski
Fernando.Mierzejewski@milliman.com

Jan Thiemen Postema
JanThiemen.Postema@milliman.com

Thomas van der Valk
Thomas.vanderValk@milliman.com

Menno van Wijk
Menno.vanWijk@milliman.com

ENDNOTES

1. Depresión aislada en niveles altos, or isolated depression at high levels.
2. Reuters. (November 8, 2024). Spain records rainiest October ever, culminating in deadly floods. Retrieved December 1, 2025, from https://www.reuters.com/world/europe/spain-records-rainiest-october-ever-culminating-deadly-floods-2024-11-08/.
3. Munich Re. (January 9, 2025). Climate change is showing its claws: The world is getting hotter, resulting in severe hurricanes, thunderstorms and floods. Retrieved December 3, 2025, from https://www.munichre.com/en/company/media-relations/media-information-and-corporate-news/media-information/2025/natural-disaster-figures-2024.html.
4. European Centre for Medium-Range Weather Forecasts. (January 2025). Severe rain in central Europe from Storm Boris. Retrieved December 3, 2025, from https://www.ecmwf.int/en/newsletter/182/news/severe-rain-central-europe-storm-boris.
5. Munich Re NatCatSERVICE. (January 2025). Natural disasters in 2024. Retrieved December 3, 2025, from https://www.munichre.com/content/dam/munichre/mrwebsitespressreleases/MunichRe-NatCAT-Stats2024-Full-Year-Factsheet.pdf/_jcr_content/renditions/original./MunichRe-NatCAT-Stats2024-Full-Year-Factsheet.pdf.
6. Prida, A. (September 22, 2021). 2021 European Summer Floods: A warning about the climate-induced increase in flood risk? AXA Climate. Retrieved December 1, 2025, from https://climate.axa/publications/2021-european-summer-floods-a-warning-about-the-climate-induced-increase-in-flood-risk/.
7. Munich Re. (January 10, 2022). Hurricanes, cold waves, tornadoes: Weather disasters in USA dominate natural disaster losses in 2021. Retrieved December 3, 2025, from https://www.munichre.com/en/company/media-relations/media-information-and-corporate-news/media-information/2022/natural-disaster-losses-2021.html.
8. Milliman. (n.d.). Extreme weather events in Europe. Retrieved December 1, 2025, from https://www.milliman.com/en/insight/extreme-weather-events-in-europe-2021.
9. Coles, S. (2001). An introduction to statistical modeling of extreme values. Springer.
10. Fisher-Tippett-Gnedenko theorem. (n.d.). Wikipedia. Retrieved December 1, 2025, from https://en.wikipedia.org/wiki/Fisher%E2%80%93Tippett%E2%80%93Gnedenko_theorem.
11. Pickands-Balkema-De Haan theorem. (n.d.). Wikipedia. Retrieved December 1, 2025, from https://en.wikipedia.org/wiki/Pickands%E2%80%93Balkema%E2%80%93De_Haan_theorem.
12. Available at https://www.ncei.noaa.gov/products/land-based-station/global-historical-climatology-network-daily.
13. Beersma, J., Hakvoort, H., Jilderda, R., Overeem, A., & Versteeg, R. (2019). Neerslagstatistiek en -reeksen voor het waterbeheer 2019. STOWA. Retrieved December 1, 2025, from https://www.stowa.nl/sites/default/files/assets/PUBLICATIES/Publicaties%202019/STOWA%202019-19%20neerslagstatistieken.pdf.
14. Wijngaard, J. B., Klein Tank, A. M. G., & Können, G. P. (2003). Homogeneity of 20th century European daily temperature and precipitation series. International Journal of Climatology, 23(6), 679–692. Retrieved December 1, 2025, from https://rmets.onlinelibrary.wiley.com/doi/abs/10.1002/joc.906.
15. Kolmogorov-Smirnov test. (n.d.). Wikipedia. Retrieved December 1, 2025, from https://en.wikipedia.org/wiki/Kolmogorov%E2%80%93Smirnov_test.
16. Cramér-von Mises criterion. (n.d.). Wikipedia. Retrieved December 1, 2025, from https://en.wikipedia.org/wiki/Cram%C3%A9r%E2%80%93von_Mises_criterion.
17. Clauset, A., Shalizi, C. R., & Newman, M. E. J. (2007). Power-law distributions in empirical data. Retrieved December 1, 2025, from https://arxiv.org/abs/0706.1062.
18. Voitalov, I., Van Der Hoorn, P., Van Der Hofstad, R., & Krioukov, D. (2019). Scale-free networks well done. Physical Review Research, 1(3), 033034. Retrieved December 1, 2025, from https://journals.aps.org/prresearch/pdf/10.1103/PhysRevResearch.1.033034.
19. Available at https://cran.r-project.org/web/packages/ismev/index.html.
20. Coles, S. (2001). An introduction to statistical modeling of extreme values. Springer.
21. A return period is the average time between occurrences of an event of certain magnitude. The return level is, in our application, the level of precipitation associated with that event.
22. This concerns the weather station “Valencia” in Valencia, not the Turis or Oliva weather stations referred to earlier.
23. BBC. (November 4, 2024). Watch: Barcelona airport and highways hit by flooding [Video]. Retrieved December 1, 2025, from https://www.bbc.com/news/videos/c937l4965v0o.
24. Consolidated text: Commission Delegated Regulation (EU) 2015/35 of 10 October 2014 supplementing Directive 2009/138/EC of the European Parliament and of the Council on the taking-up and pursuit of the business of Insurance and Reinsurance (Solvency II) (Text with EEA relevance). Retrieved December 1, 2025, from https://eur-lex.europa.eu/eli/reg_del/2015/35.